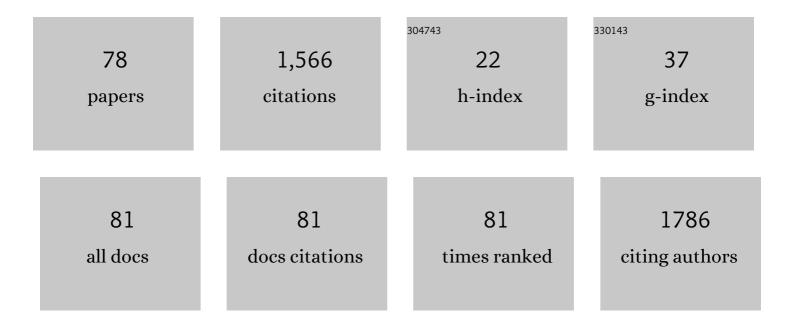
List of Publications by Year in descending order

Source: https://exaly.com/author-pdf/7631055/publications.pdf Version: 2024-02-01



#	Article	IF	CITATIONS
1	Structure, composition and optical properties of Cu2ZnSnS4 thin films deposited by Pulsed Laser Deposition method. Solar Energy Materials and Solar Cells, 2011, 95, 2907-2913.	6.2	176
2	Solution-processed SnO2 interfacial layer for highly efficient Sb2Se3 thin film solar cells. Nano Energy, 2019, 60, 802-809.	16.0	111
3	Modulated photoluminescence spectroscopy with a step-scan Fourier transform infrared spectrometer. Review of Scientific Instruments, 2006, 77, 063104.	1.3	105
4	Comprehensive understanding of heat-induced degradation of triple-cation mixed halide perovskite for a robust solar cell. Nano Energy, 2018, 54, 218-226.	16.0	72
5	Broadband Bi ₂ O ₂ Se Photodetectors from Infrared to Terahertz. Advanced Functional Materials, 2021, 31, 2009554.	14.9	65
6	Origin of Band-Tail and Deep-Donor States in Cu ₂ ZnSnS ₄ Solar Cells and Their Suppression through Sn-Poor Composition. Journal of Physical Chemistry Letters, 2019, 10, 7929-7936.	4.6	64
7	Influence of annealing temperature on structural and optical properties of Cu2MnSnS4 thin films fabricated by sol–gel technique. Journal of Alloys and Compounds, 2015, 640, 23-28.	5.5	53
8	Comparative study on Cu2ZnSnS4 thin films deposited by sputtering and pulsed laser deposition from a single quaternary sulfide target. Journal of Crystal Growth, 2012, 361, 147-151.	1.5	52
9	Photoreflectance spectroscopy with a step-scan Fourier-transform infrared spectrometer: Technique and applications. Review of Scientific Instruments, 2007, 78, 013111.	1.3	47
10	High-speed ultraviolet photodetectors based on 2D layered CuInP2S6 nanoflakes. Applied Physics Letters, 2020, 117, .	3.3	42
11	Photomodulated infrared spectroscopy by a step-scan Fourier transform infrared spectrometer. Applied Physics Letters, 2006, 89, 182121.	3.3	32
12	Oxygen-vacancy-related dielectric relaxation in BiFeO3films grown by pulsed laser deposition. Journal Physics D: Applied Physics, 2008, 41, 215403.	2.8	30
13	Electric-Field-Induced Room-Temperature Antiferroelectric–Ferroelectric Phase Transition in van der Waals Layered GeSe. ACS Nano, 2022, 16, 1308-1317.	14.6	30
14	A flexible polypyrrole/silk-fiber ammonia sensor assisted by silica nanosphere template. Sensors and Actuators A: Physical, 2021, 317, 112436.	4.1	29
15	Temperature dependence of optical band gap in ferroelectric Bi3.25La0.75Ti3O12 films determined by ultraviolet transmittance measurements. Applied Physics Letters, 2007, 91, .	3.3	28
16	Deep/shallow levels in arsenic-doped HgCdTe determined by modulated photoluminescence spectra. Applied Physics Letters, 2008, 93, 131909.	3.3	28
17	Modulated photoluminescence of shallow levels in arsenic-doped Hg1â^'xCdxTeâ€^(xâ‰^0.3) grown by molecular beam epitaxy. Applied Physics Letters, 2008, 92, .	3.3	28
18	Room temperature preparation of highly stable cesium lead halide perovskite nanocrystals by ligand modification for white light-emitting diodes. Nano Research, 2021, 14, 2770-2775.	10.4	28

#	Article	IF	CITATIONS
19	A "Turn-on―fluorescence perovskite sensor based on MAPbBr3/mesoporous TiO2 for NH3 and amine vapor detections. Sensors and Actuators B: Chemical, 2021, 327, 128918.	7.8	26
20	Anomalous temperature dependence of absorption edge in narrow-gap HgCdTe semiconductors. Applied Physics Letters, 2006, 89, 021912.	3.3	25
21	Investigation of Cu2ZnSnS4 thin films with controllable Cu composition and its influence on photovoltaic properties for solar cells. Journal of Alloys and Compounds, 2017, 694, 833-840.	5.5	25
22	Effect of CZTS/CdS interfaces deposited with sputtering and CBD methods on Voc deficit and efficiency of CZTS solar cells. Journal of Alloys and Compounds, 2020, 817, 153329.	5.5	23
23	Efficient Er/Oâ€Doped Silicon Lightâ€Emitting Diodes at Communication Wavelength by Deep Cooling. Advanced Optical Materials, 2020, 8, 2000720.	7.3	23
24	Stable fluorescent NH3 sensor based on MAPbBr3 encapsulated by tetrabutylammonium cations. Journal of Alloys and Compounds, 2020, 835, 155386.	5.5	23
25	PbS:Glass as broad-bandwidth near-infrared light source material. Optics Express, 2013, 21, 2287.	3.4	20
26	Atomic Insights into Ti Doping on the Stability Enhancement of Truncated Octahedron LiMn2O4 Nanoparticles. Nanomaterials, 2021, 11, 508.	4.1	18
27	Magnetophotoluminescence study of GaxIn1â^'xP quantum wells with CuPt-type long-range ordering. Journal of Applied Physics, 2006, 100, 053522.	2.5	16
28	Properties of highly (100) oriented Pb(Mg1â^•3,Nb2â^•3)O3–PbTiO3 films on LaNiO3 bottom electrodes. Applied Physics Letters, 2007, 91, .	3.3	16
29	Influence of substitution of Nd3+ for Bi3+ on structure and piezoelectric properties of SrBi2â´Ĩ‡Ndl‡Nb2O9 (l‡=0, 0.1, 0.2 and 0.4). Transactions of Nonferrous Metals Society of China, 2009, 19, 1459-1463.	4.2	16
30	Positive Role of Inhibiting CZTSSe Decomposition on Intrinsic Defects and Interface Recombination of 12.03% Efficient Kesterite Solar Cells. Solar Rrl, 2022, 6, .	5.8	16
31	Effect of thickness on the dielectric property and nonlinear current–voltage behavior of CaCu3Ti4O12 thin films. Physics Letters, Section A: General, Atomic and Solid State Physics, 2009, 373, 2389-2392.	2.1	15
32	Spontaneous and stimulated emission dynamics of PbS quantum dots in a glass matrix. Physical Review B, 2013, 87, .	3.2	15
33	Cutoff wavelength of Hg1â^xCdxTe epilayers by infrared photoreflectance spectroscopy. Applied Physics Letters, 2007, 90, 171101.	3.3	14
34	Synthesis and characterization of Cu-based selenide photovoltaic materials: Cu2FeSnSe4 and Cu(In,) Tj ETQq0 0	0 rgBT /O	verlock 10 Tf

35	Compositional dependence of photovoltaic properties of Cu2ZnSnSe4 thin film solar cell: Experiment and simulation. Solar Energy, 2018, 159, 572-578.	6.1	13
36	Thin-wall cyclic olefin copolymer tube waveguide for broadband terahertz transmission. Optical Materials, 2019, 98, 109490.	3.6	13

#	Article	IF	CITATIONS
37	Investigation of microstructural and optical properties of Cu(In, Al)Se 2 thin films with various copper content. Journal of Alloys and Compounds, 2015, 651, 208-213.	5.5	12
38	Stimulated emission from PbSâ€quantum dots in glass matrix. Laser and Photonics Reviews, 2013, 7, L1.	8.7	11
39	Preparation and transmission characteristics of a mid-infrared attenuated total reflection hollow waveguide based on a stainless steel capillary tube. Applied Optics, 2016, 55, 6404.	2.1	11
40	Optical homogeneity analysis of Hg 1â°'x Cd x Te epitaxial layers: How to circumvent the influence of impurity absorption bands?. Infrared Physics and Technology, 2017, 82, 1-7.	2.9	11
41	Preparation and characterization of BiFeO3/LaNiO3 heterostructure films grown on silicon substrate. Journal of Crystal Growth, 2010, 312, 617-620.	1.5	10
42	Strategic improvement of Cu2SnS3 thin film by different heating rates and photoluminescence investigation. Materials Science in Semiconductor Processing, 2018, 84, 124-130.	4.0	10
43	Temperature dependence of the fundamental excitonic resonance in lead-salt quantum dots. Applied Physics Letters, 2015, 107, .	3.3	9
44	The synthesis and microstructural, optical, magnetic characterizations of m 0 0-oriented epitaxial Bi 2 Fe 4 O 9 thin film by pulsed laser deposition. Materials Letters, 2017, 204, 81-84.	2.6	9
45	A flexible paper sensor based on polyaniline/germanium film for NH3 detection. Materials Letters, 2020, 278, 128438.	2.6	9
46	Stimulated emission at 1.54  μm from erbium/oxygen-doped silicon-based light-emitting diodes. Photo Research, 2021, 9, 714.	nics 7.0	9
47	Effects of deposition temperature and post-annealing on structure and electrical properties in (La0.5Sr0.5)CoO3 films grown onÂsilicon substrate. Applied Physics A: Materials Science and Processing, 2009, 95, 721-725.	2.3	8
48	Antimony-induced grain growth and properties modification of Cu(In, Al)Se2 thin films fabricated by selenization of sputtered stacked precursors. Journal of Alloys and Compounds, 2016, 689, 21-29.	5.5	8
49	Thermal behaviors of stainless steel tube based GeO 2 ATR hollow fibers for transmitting CO 2 laser radiations. Optics and Laser Technology, 2017, 95, 42-45.	4.6	8
50	Short-wavelength infrared defect emission as a probe of degradation processes in 980 nm single-mode diode lasers. Laser and Photonics Reviews, 2014, 8, L59-L64.	8.7	7
51	MGa ₂ B ₂ O ₇ :Bi ³⁺ ,Al ³⁺ (M = Sr, Ba) blue phosphors with a quantum yield of 99% and negative thermal quenching. Inorganic Chemistry Frontiers, 2021, 8, 4257-4266.	6.0	7
52	Electric-field modulated photovoltaic effect of ferroelectric double-perovskite Bi2FeMnO6 films. Applied Physics Letters, 2021, 119, .	3.3	7
53	Experimental observation of exciton splitting and relaxation dynamics from PbS quantum dots in a glass matrix. Physical Review B, 2014, 89, .	3.2	6
54	Growth and ellipsometric characterizations of highly (111)-oriented Bi2Ti2O7 films on platinized silicon by metal organic decomposition method. Journal of Vacuum Science and Technology A: Vacuum, Surfaces and Films, 2008, 26, 1287-1292.	2.1	5

#	Article	IF	CITATIONS
55	Influence of annealing conditions on impurity species in arsenic-doped HgCdTe grown by molecular beam epitaxy. Chinese Physics B, 2010, 19, 117106.	1.4	5
56	Microstructure tuning and magnetism switching of ferroelectric barium titanate. Materials Characterization, 2015, 107, 1-6.	4.4	5
57	Structural and optical tunability by reaction time of selenization in Cu2FeSnSe4 thin films. Journal of Alloys and Compounds, 2015, 646, 68-72.	5.5	5
58	Phase transitions and electrical/optical properties in (1-x)KNbO3-x(Ba0.5Bi0.5)(Nb0.5Zn0.5)O3 ceramics. Ceramics International, 2020, 46, 18026-18031.	4.8	5
59	Influence of selenium growth condition on the photovoltaic conversion efficiency of Sb2Se3 as the solar cell absorption layer. Journal of Materials Science: Materials in Electronics, 2022, 33, 10335-10342.	2.2	4
60	Synthesis, Structure and Properties of Formamidineâ€ŧemplated Metal Formate Crystals. Crystal Research and Technology, 2017, 52, 1700195.	1.3	3
61	Metallic hollow waveguide based on GeO2–NaOH precursor solution for transmission of CO2 laser radiations. Optical and Quantum Electronics, 2018, 50, 1.	3.3	3
62	Carrier Transfer of Deepâ€Level Localized States in Typeâ€II In x Ga 1â^' x As/GaN y As 1â^' y Shortâ€Period Superlattice. Physica Status Solidi (B): Basic Research, 2020, 257, 1900258.	1.5	3
63	Transmission behaviors of metallic ATR mid-infrared hollow waveguide at low temperature and performance improvement. Optics Communications, 2020, 458, 124821.	2.1	3
64	Infrared emission bands and thermal effects for 440-nm-emitting GaN-based laser diodes. AIP Advances, 2020, 10, .	1.3	3
65	Broadband Photodetectors: Broadband Bi ₂ O ₂ Se Photodetectors from Infrared to Terahertz (Adv. Funct. Mater. 14/2021). Advanced Functional Materials, 2021, 31, 2170093.	14.9	3
66	Origin of yellow emissions from (In,Ga,Al)N based 450â€nm emitting diode lasers. OSA Continuum, 2019, 2, 1496.	1.8	3
67	Impurity Activation in MBE-Grown As-Doped HgCdTe by Modulated Photoluminescence Spectra. Chinese Physics Letters, 2009, 26, 047804.	3.3	2
68	Bandgap narrowing and ferroic modulation in KNbO3 ceramics composited by spinel AFe2O4 (A = Mg,) Tj ETQq	00 <u>0</u> ggBT	Oyerlock 10
69	Narrow-Gap Semiconductors and Low-Dimensional Structures for Optoelectronic Applications. Scientific World Journal, The, 2014, 2014, 1-2.	2.1	1
70	Charge character in the doubleâ€barrier quantum dots in well hybrid structure. Micro and Nano Letters, 2015, 10, 533-536.	1.3	1
71	Short-wavelength infrared defect emission as probe for degradation effects in diode lasers. , 2015, , .		1

#	Article	IF	CITATIONS
73	Electromagnetic wave propagation and heat radiative effect in metal particle cloud. , 2006, , .		О
74	The determination of the <i>x</i> value in doped Hg _{1â^'<i>x</i>} Cd _{<i>x</i>} Te by transmission spectra. Chinese Physics B, 2012, 21, 017804.	1.4	0
75	Thermal oxidation-resistant GeO2 ATR hollow waveguide based on NiCr capillary tube and its thermal effects. Applied Physics B: Lasers and Optics, 2018, 124, 1.	2.2	0
76	NIR-Emitting Erbium/Oxygen-Doped Silicon by Self-Assembled Techniques. , 2019, , .		0
77	Field dependent ultrafast carrier dynamics in InGaN/GaN p-i(MQW)-n structure. Superlattices and Microstructures, 2020, 137, 106354.	3.1	0
78	Ferro-electric and magnetic properties in Bi ₅ Ti ₃ FeO ₁₅ films by Mn doping. Journal of Materials Chemistry C, 2022, 10, 1003-1009.	5.5	0